Supporting Information

ZrB_2-based "Brick-and-Mortar" Composites Achieving the Synergy of Superior Damage Tolerance and Ablation Resistance

Yehong Cheng[1,2], Yumin An[1], Yaxiong Liu[1], Qiang Wei[1,2], Wenbo Han[3], Xinghong Zhang[3], Peng Zhou[4*], Chuncheng Wei[5*], Ning Hu[6,1*]

[1]School of Mechanical Engineering, Hebei University of Technology, Tianjin, 300401, P.R. China.

[2]Research Institute for Structure Technology of Advanced Equipment, Hebei University of Technology, Tianjin, 300401, P.R. China.

[3]National Key Laboratory of Science and Technology on Advanced Composites in Special Environments, Harbin Institute of Technology, Harbin, 150080, P.R. China.

[4]Institute of intelligent manufacturing technology, Shenzhen Polytechnic, Shenzhen, 518055, P.R. China.

[5]School of Material Science and Engineering, Shandong University of Technology, Zibo, 255049, P.R. China.

[6]State Key Laboratory of Reliability and Intelligence Electrical Equipment, Hebei University of Technology, Tianjin, 300401, P.R. China.

*Corresponding authors. E-mail: Peng Zhou (975201937@qq.com); Chuncheng Wei (chun_cheng@sdut.edu.cn); Ning Hu (ninghu@hebut.edu.cn).

1. Material preparation and Measurement

Photographs of the ZS/ZSG "brick-and-mortar" ceramics during the fabrication process are presented in Figure S1. The continuous ZS/ZSG fibers were collected, as presented in Figure S1(a). Figure S1(b) presents the axially aligned fiber sheets obtained via directional uniaxial alignment, and then cut into discs to receive ceramic fiber discs, as shown in Figure S1(c). ZS/ZSG ceramic green body was obtained by assembling ceramic fiber discs with preset twist angles from bottom to top, as presented in Figure S1(d), and then pre-pressed in a graphite mold. Finally, ZS/ZSG "brick-and-mortar" ceramic billet with size of Φ50 mm × 6 mm was obtained by vacuum degreasing and hot-pressing, as shown in Figure S1(e).

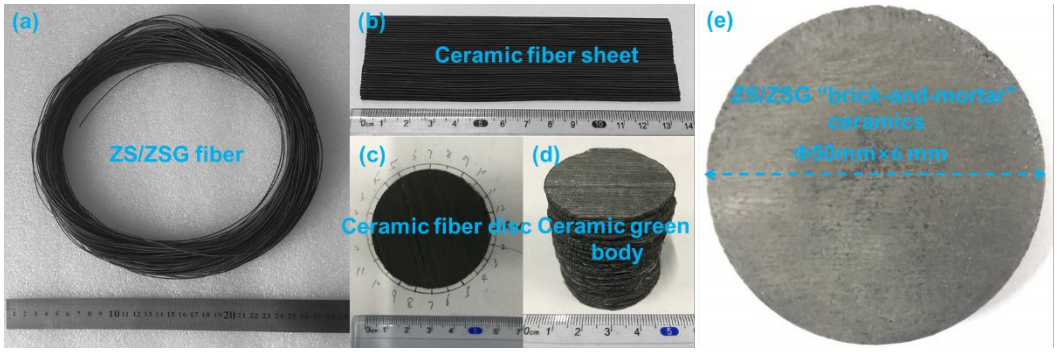

Figure S1. Physical photographs of ZS/ZSG "brick-and-mortar" ceramics during fabrication process: (a) ZS/ZSG fiber, (b) axially aligned ceramic fiber sheet, (c) ceramic fiber disc, (d) ceramic green body, (e) ZS/ZSG "brick-and-mortar" ceramic billet.

The three-point bending bars were cut along the fiber alignment direction. The size of flexural strength sample is 3 mm × 4 mm × 36 mm, the 4 mm × 36 mm planes lie in laminated plane. The size of single-edge V-shaped notched beams is 2 mm × 4 mm ×22 mm, the 2 mm × 22 mm planes parallel to laminated plane. The locations of three-point bending bars in "brick-and-mortar" ceramics billets are shown in Figure S2. The surface microstructure of 3 mm × 36 mm or 4 mm × 22 mm planes are presented in Figure 2, and Figure 3 shows the fracture surface of 3 mm ×4 mm planes in flexural strength bars or 2 mm × 4 mm planes in single-edge V-shaped notched beams.

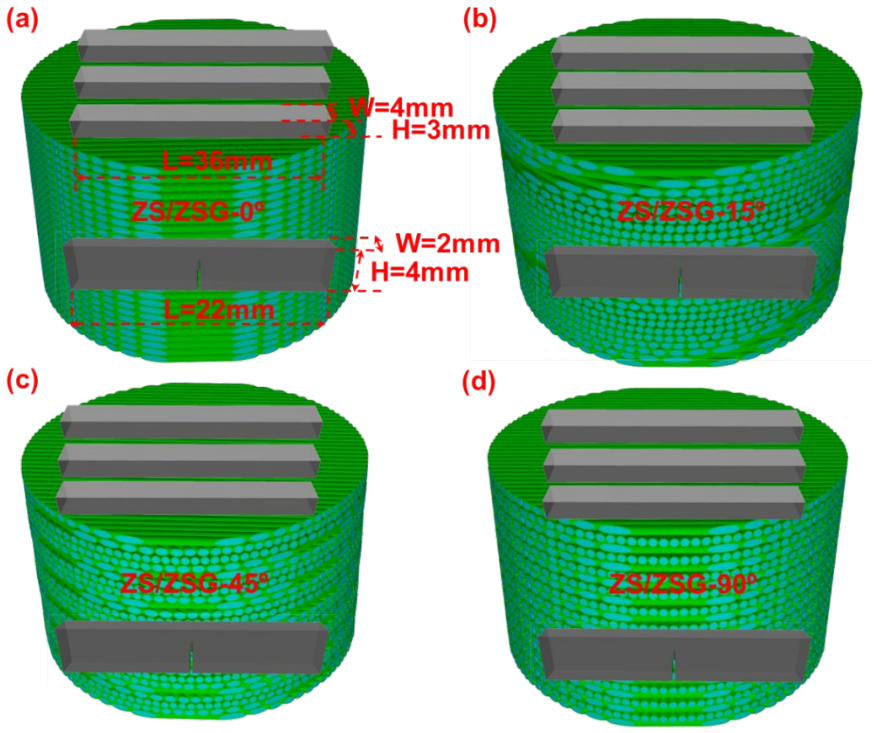

Figure S2. Locations of three-point bending bars in "brick-and-mortar" ceramic billets.

The sample preparation of flexural strength was according to the state standard of China (GB/T 6569-2006/ISO 14704:2000) for fine ceramics (advanced ceramics, advanced technical ceramics). All test bars shall be ground to achieve the desired roughness. 200# sandpaper was firstly used for rough grinding, then 600# sandpaper was used for fine grinding and chamfering along 45° deviating from the long edges with a depth of about 0.1mm. Finally, 1000# sandpaper has been used to polish the surface and chamfering surface.

2. Elemental distribution of ZS/ZSG "brick-and-mortar" ceramics

The scanning electron image and element distribution of ZS/ZSG-15º ceramics are shown in Figure S3. The dark gray ZrB_2-SiC matrix phase was wrapped by grey ZrB_2-SiC-rGO interface phase, as presented in Figure S3(a). The relative content and distribution of Zr, Si and C elements can be clearly distinguished from the surface element distribution in Figure S3(b)-(d). Color level is located on the upper-right corner of the figures, the color represents the relative contents of elements in element scanning micrographs. The green color is above the blue color, which indicates the Zr element

content in the green cell is greater than that of Zr element in the blue cell boundary, as shown in Figure S3(b), which is ascribed to the content of Zr in the matrix (ZrB_2-20vol.%SiC) is higher than that of the interface phase (ZrB_2-20vol.%SiC-30vol.%rGO). Similarly, the relative content of Si element in matrix is higher than that of interface, and the Si element appears in black color at the interface, as shown in Figure S3(c). The light blue color is above the dark blue color, which indicates that the content of C element in the light blue cell boundary is higher than that in the dark blue cell, because the rGO is enriched at the weak interface, as shown in Figure S3(d).

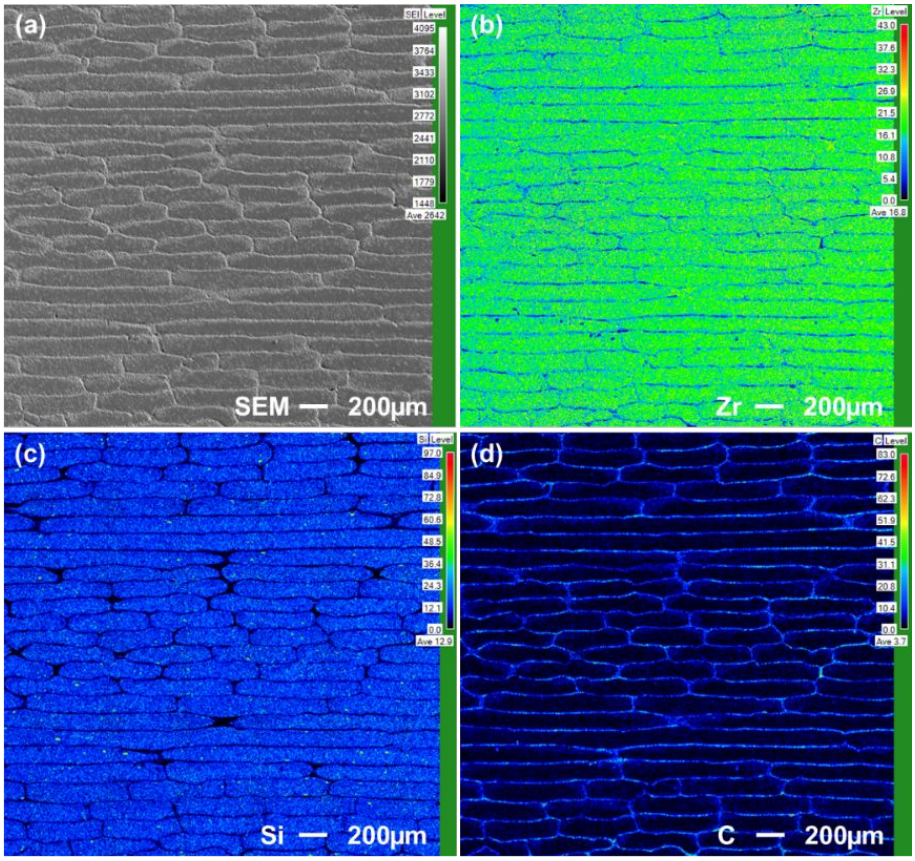

Figure S3. SEM and elemental distribution in ZS/ZSG-15º "brick-and-mortar" ceramics, (a) SEM, element scanning micrographs of (b) Zr, (c) Si and (d) C elements.

3. Microstructures of ZrB_2-SiC and ZrB_2-SiC-rGO layers

High magnification images of ZrB_2-SiC and ZrB_2-SiC-rGO layers are presented in Figure S4. The ZrB_2-SiC layer exhibits densified microstructure, the black grain is SiC and the grey is ZrB_2 matrix, and the smaller SiC grains distribute uniformly in larger ZrB_2 grains, as shown in Figure S4(a). The rGO nanosheets distributed in ZrB_2-SiC-rGO

layer and the obvious extraction of rGO sheets was observed in Figure S4(b).

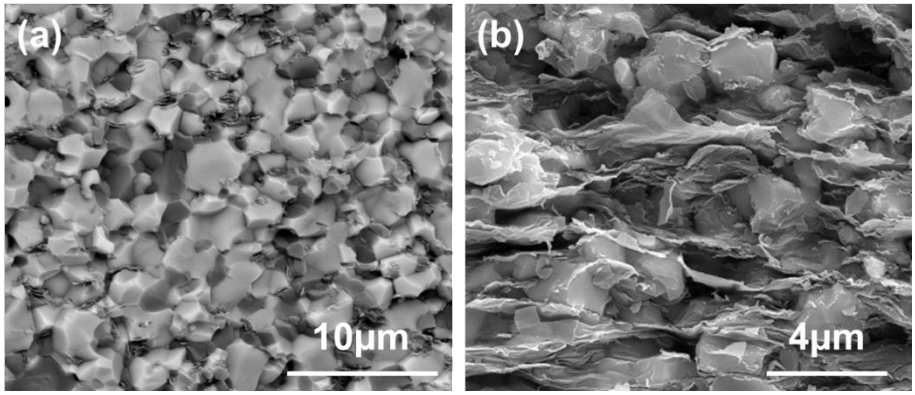

Figure S4. High magnification images of ZrB_2-SiC and ZrB_2-SiC-rGO layers, (a) backscattered electron image of ZrB_2-SiC and (b) SEM of ZrB_2-SiC-rGO layer.

4. Microstructure and mechanical property of ZS/ZSG-0º cut at 90° deviation from axial orientation

To investigate the in-plane anisotropic properties of uniaxially aligned ZS/ZSG-0º "brick-and-mortar" ceramics, samples were taken 90º off axial orientation (perpendicular to the fiber axis), it can be observed that each fiber is compressed into a rectangular strip from the cross section, as shown in Figure S5(a), the width of the ZrB_2-SiC laminate is about 600 μm and the height is about 230 μm. The fracture morphology of the ZS/ZSG-0º sample taken at 90º from the fiber axis is shown in Figure S5(b), and the fracture surface is composed of uneven fibers arranged parallel in one direction. Figure S5(c) shows the crack propagation path of the ZS/ZSG-0º deviating from 90º off from the axial direction, and the crack continuously deflected along the weak interface of ZrB_2-SiC-rGO. The crack propagates along the straight line in the ZrB_2-SiC region until the next ZrB_2-SiC-rGO interface is encountered and deflection again occurs until the crack extends to the edge of the sample.

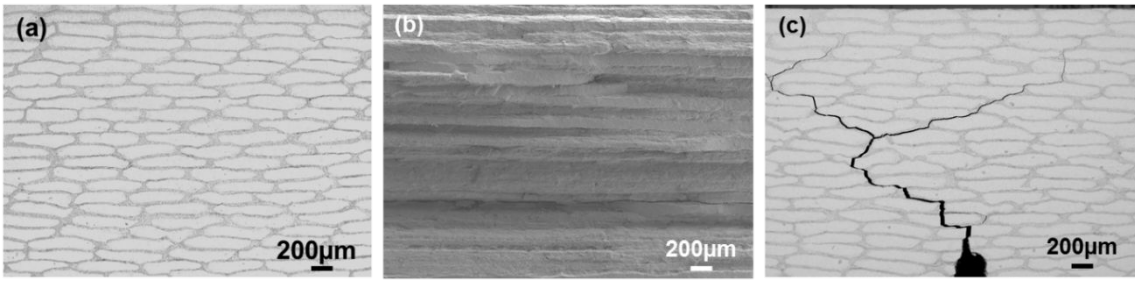

Figure S5. (a) Cross-section microstructure, (b) fracture microstructure and (c) crack propagation paths of ZS/ZSG-0º tested at 90° off axial orientation.

Table S1. Relative density (ρ), elastic modulus (E), flexural strength (σ), fracture toughness (K_{IC}) and work of fracture (γ_{WOF}) of ZS/ZSG-0º tested at 90º off axial orientation (ZS/ZSG-0º off 90º)

Composition	ρ (%)	E (GPa)	σ (MPa)	K_{IC} SEVNB (MPa·m$^{1/2}$)	γ_{WOF} (J/m^2)
ZS/ZSG-0º off 90º	95.2	323 ± 5	180 ± 15	4.34 ± 0.11	195.3 ± 42.3

5. Grain size distribution

The grain size distribution of ZS/ZSG "brick-and-mortar" ceramics are presented in Figure S6. The average grain size of ZS/ZSG "brick-and-mortar" ceramics are about 3.65 μm, 3.28 μm, 3.50 μm and 3.42 μm, respectively. The grain size distribution conforms to normal distribution, there are two peaks in the grain size distribution which correspond to the highest fraction of ZrB_2 and SiC grain. No obvious variation existed in grain size.

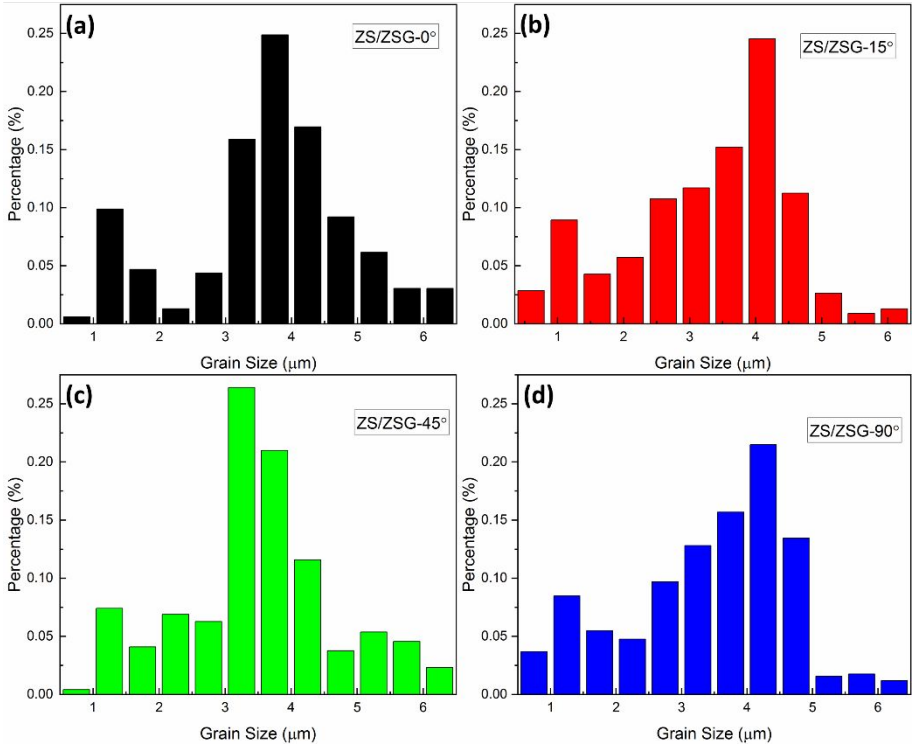

Figure S6. Size distributions of grains measured in ZS/ZSG "brick-and-mortar" ceramics: (a) ZS/ZSG-0º, (b) ZS/ZSG-15º, (c) ZS/ZSG-45º and (d) ZS/ZSG-90º

6. Microstructure of V-notches for ZS/ZSG “brick-and-mortar” ceramics

The traditional blade cutting method for preparing V-shaped incisions has poor size uniformity and wide notches. In this work, nano laser processing technology was carried out to prefabricated sharp V-notches. Nanosecond laser grooving was performed on a fiber laser marking machine from Xindazu Laser Equipment Co., Ltd., Heilongjiang Province, China. Processing parameters: laser wavelength is 1046nm, pulse width is 10ns, output power is 10W, scanning speed is 50 mm/s, processing time is 50 times. The notches prepared by this method is sharper than the that prepared by the blade grooving method. By adjusting the laser processing parameters, it is possible to prepare V-notches with various depths and tip radii. The microstructure of V-notches was provided in Figure S7, sharp V-shaped notches with tip radius of ~2.5 μm were etched via laser at the bottom of the U-shaped grooves of single-edge notched beams (SENBs). The V-notches have better uniformity and stability in size, and the tip radius V-notches value is far below the critical tip radius of ZrB_2-based ceramics according to previous work (J. Eur. Ceram. Soc. 37 (2017) 4207-4212).

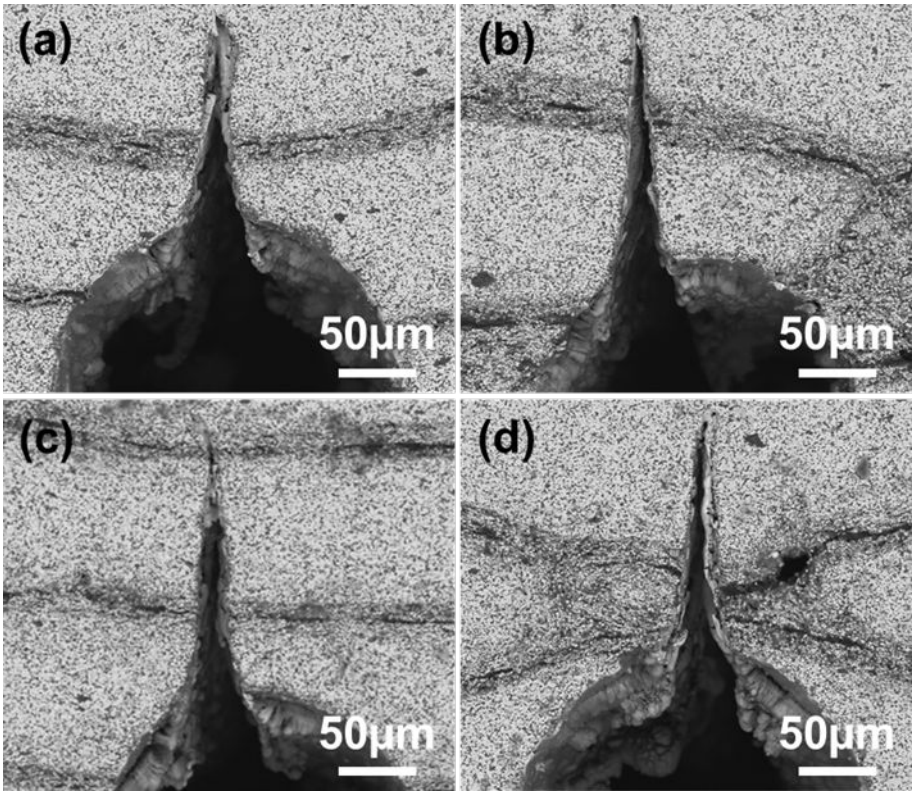

Figure S7. Microstructure of V-notches for (a) ZS/ZSG-0º, (b) ZS/ZSG-15º, (c) ZS/ZSG-45º, and (d) ZS/ZSG-90º “brick-and-mortar” ceramics.

7. Oxy-acetylene ablation

The sizes of in-plane and out-plan ablating samples are about 10 mm × 5 mm × 6 mm (Length × Width × Thickness) and 10 mm × 6 mm × 10 mm (Length × Width × Thickness), respectively. The in-plane direction is parallel to laminated plane, and the out-plane direction is perpendicular to laminated plane, as shown in Figure S8(a). The oxy-acetylene flame was focus on the center of ablating samples. Physical photos of the ablating samples after ablation test are presented in Figure S8(b) and S8(c). The ablation samples can keep their shapes intact after oxyacetylene ablation.

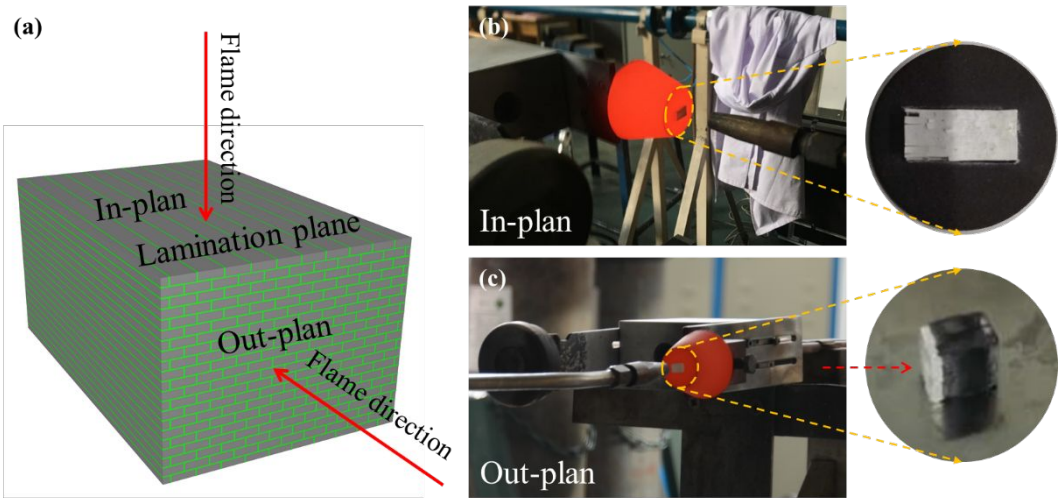

Figure S8. (a) The in-plane and out-plan direction of oxy-acetylene ablating samples, (b) and (c) physical photos of the ablating samples after ablation test.

8. Calculation of ablation rates

The mass ablation and linear ablation rates are calculated using Eqs. (1) and (2):

$$R_m = \frac{m_0 - m_1}{S \cdot t} \tag{1}$$

$$R_L = \frac{d_0 - d_1}{t} \tag{2}$$

where m_0 and m_1 are the weights of the specimen before and after ablation, respectively; d_0 and d_1 are the thickness of the specimen before and after ablation; S is the surface area of the ablation sample, and t is the ablation time.

9. Calculation of mechanical properties

The formula for calculating the work of fracture (γ_{WOF}) can be described by Eq. (3):

$$\gamma_{WOF} = \frac{W}{2A} \tag{3}$$

Where W is the application of the area under the load-displacement curve during the entire rupture of SEVNB, and A is the unnotched area of the cross section in the SEVNB sample.

The crack initiation fracture toughness (K_{IC}) is calculated by Eq. (4):

$$K_{IC} = Y \frac{3PL}{2BW^2} \sqrt{a} \tag{4}$$

Where P is the maximum load when the specimen fractures, N； L is support span，mm； B is the width of the sample, W is thickness of sample, a is the initial notch depth of the specimen, L/W=4 ， $0.35 \leqslant a/W \leqslant 0.6$. Y is the dimensionless coefficient determined by the crack shape, size and load form, which is calculated by Eq. (5):

$$Y = 1.93 - 3.07(\frac{a}{w}) + 14.53(\frac{a}{w})^2 - 25.11(\frac{a}{w})^3 + 25.80(\frac{a}{w})^4 \tag{5}$$

The crack-resistance curves (R-curve) are calculated based on J integral and SEVNB tests. The converted stress intensity factor (crack-growth fracture toughness) K_{Jc} is determined by Eq. (6):

$$K_{Jc} = (J \cdot E)^{1/2} \tag{6}$$

According to ASTM standard E1820-06 (S3), the J value is calculated according to the applied load and the instantaneous crack length, wherein the J integral includes the elastic deformation and the inelastic deformation of the material, which are calculated by Eq. (7):

$$J = J_{el} + J_{pl} \tag{7}$$

Where J_{el} and J_{pl} are calculated by Eq. (8) and Eq. (9), respectively.

$$J_{el} = \frac{K_{IC}^2}{E'} \tag{8}$$

$$J_{pl} = \frac{2A_{pl}}{B(W-a)} \tag{9}$$

Where B is the width of the sample, W is thickness of sample, a is the initial notch depth of the specimen. The relationship between E' and E can be calculated by Eq. (10).

$$E' = E(1-\nu^2) \quad (10)$$

As the variation of E influence K_{Jc} in a fairly limited way; here, E′ can be replaced by E. According to the recursive method reported in the literature [1-4], the crack propagation dimension Δa is calculated by the Eqs. (11-13).

$$a_n = a_{n-1} + \frac{W - a_{n-1}}{2}\frac{C_n - C_{n-1}}{C_n} \quad (11)$$

$$C_n = \frac{u_n}{f_n} \quad (12)$$

$$\Delta a = a_n - a \quad (13)$$

Where a_n is crack propagation length, C_n is the yield coefficient at each point after crack propagation, U_n is displacement at each point after crack propagation, f_n is the pressure at each point after crack propagation and W is the thickness of sample.

References

1. F. Bouville, E. Maire, S. Meille, B.V. Moortèle, Stevenson A.J., Deville S. Strong, tough and stiff bioinspired ceramics from brittle constituents, Nat. Mater. 13 (2014) 508-514.

2. V. Naglieri, B. Gludovatz, A.P. Tomsia, R.O. Ritchie. Developing strength and toughness in bio-inspired silicon carbide hybrid materials containing a compliant phase, Acta Mater. 98 (2015) 141-151.

3. Gao H, Chen S, Mao L, et al. Mass production of bulk artificial nacre with excellent mechanical properties[J]. Nature Communications, 2017, 8(1): 287-287.

4. E. Munch, M.E. Launey, D.H. Alsem, E. Saiz, A.P. Tomsia, R.O. Ritchie, Tough, bio-inspired hybrid materials, Science 322 (2008) 1516-1520.